Desalination and Water Treatment
www.deswater.com
doi: 10.1080/19443994.2014.979445

57 (2016) 1927–1939
January

Taylor & Francis
Taylor & Francis Group

Development of ceramic membranes from low-cost clays for the separation of oil–water emulsion

Kanchapogu Suresh, G. Pugazhenthi*

Department of Chemical Engineering, Indian Institute of Technology Guwahati, Guwahati 781039, Assam, India, Tel. +91 361 2582264; Fax: +91 361 2582291; email: pugal@iitg.ernet.in (G. Pugazhenthi)

Received 9 March 2014; Accepted 16 October 2014

ABSTRACT

This work addresses the fabrication of ceramic microfiltration membranes by uniaxial dry compaction method. Four membranes, namely SP1, SP2, SP3, and SP4 were prepared with various compositions of fly ash and titanium dioxide (TiO_2) followed by sintering at 1,100˚C. The raw materials and the prepared membranes were characterized by particle size distribution, X-ray diffraction and field emission scanning electron microscope, porosity, pore size, and chemical and mechanical stabilities. As the TiO_2 content increases in the precursor formulations, the porosity and mechanical stability of the membranes also increase while the average pore size reduces from 2.97 to 1.32 μm. The chemical stability of all the membranes demonstrates to be better in both acidic and basic medium. The performance of the membrane (SP4) is examined for the separation of oil–water emulsion and the membrane exhibits a maximum oil rejection of 99.2%.

Keywords: Fly ash; TiO_2; Ceramic membrane; Oil–water emulsion

1. Introduction

In recent years, ceramic membrane-based separation processes have been recognized for treating liquid-phase solution because of its advantages including high chemical, mechanical, and thermal stabilities and higher separation efficiency [1–5]. The key factor for the membrane separation process is the selection of membrane that comprises better chemical, mechanical, and thermal stabilities. Several literatures have demonstrated the fabrication of ceramic membranes using various raw materials such as α-alumina, γ-alumina, zirconia, TiO_2, and silica [1,2,6–10]. Conversely, the cost of these membranes is quite high because of expensive raw materials and the need for high sintering temperature (>1,300˚C) [7]. From the economic point of view, the membranes derived from the above costly raw materials are not suitable for industrial applications. To overcome these problems, presently, research is devoted to other raw materials that would be of low cost and suitable as a standard raw material replacement. Therefore, in recent times, various clays (raw clay, Moroccan clay, apatite powder, dolomite, kaolin, Tunisian clay, sepiolite clay, and Algerian clay) have been identified as best cost-effective raw materials for membrane applications [11–18]. Besides, most of the literature indicated that fly ash is a richly available waste material from coal-burning plants and this is a major threat to the environment. Therefore, it is a great challenge to find an alternative way to environmental solution to dispose fly ash. Various alternative methods were developed to utilize

*Corresponding author.

fly ash. One of the alternatives was to use fly ash as a raw material for fabrication of ceramic membranes. Recently, some researchers have attempted to exploit fly ash as a raw material for the preparation of ceramic membrane supports [19–21]. Dong et al. [20] have developed mullite supports by sintering (1,450˚C) fly ash with various amounts of titania and the average pore size of the obtained supports was in the range of 6.52–7.28 μm. In the work of Fang et al. [21], fly ash-based tubular support with an average pore size of 2.13 μm was prepared by an extrusion method and sintered at 1,190˚C.

Majorly, three techniques including extrusion, slip casting, and uniaxial pressing/compaction are widely used to fabricate ceramic microfiltration membranes (CMM). Most of the researchers have adopted slip casting and extrusion methods for the fabrication of CMM from high-purity clays and fly ash [18,21,22]. The membranes produced using these techniques usually possess higher porosity and are also expensive [22]. Hence, this study is designed to test the feasibility of preparing lower pore size membranes with good mechanical strength from industrial waste fly ash by a facile fabrication technique.

Oily wastewater produced from various industries including petroleum, metallurgical, petrochemical, transportation, and food processing must be treated before being discharged into environment owing to its toxicity and ecological hazards. These industries generate wastewater with oil concentration of 50–1,000 mg/L [23,24]. In accordance with industrial pollution norms, the maximum allowable limit of oil and grease concentration in industrial effluent is 10–15 mg/L [25–27]. The treatment of oily wastewater by conventional methods such as coagulation, de-emulsification, dissolved air floatation, flocculation, gravity separation, and skimming are not efficient, primarily when the oil concentration is low [27]. Therefore, nowadays, membrane technology is being used for the treatment of oily wastewater because of its higher separation efficiency. Presently, CMM are also escalating a large interest in the field of oily wastewater treatment [27,28]. Abadi et al. [27] have demonstrated around 95% removal of TOC from oily wastewater using tubular α-Al_2O_3 microfiltration membrane with pore size of 0.2 μm. Zhou et al. [28] have prepared the hydrophilic ZrO_2/Al_2O_3 ceramic composite membrane and used for the separation of stable oil-in-water emulsion. They achieved about 97.8% rejection of oil with good permeate flux for the feed concentration of 1,000 mg/L.

The objective of this work is to fabricate CMM with four different compositions of raw materials by uniaxial dry compaction method. The pore structural characteristics (e.g. porosity, pore size, and pore morphology) and mechanical and chemical stabilities of the membranes are also investigated. The separation potential of the membrane is tested for the separation of oil–water emulsion.

2. Materials and methods

2.1. Starting materials

The composition of raw materials used for the fabrication of ceramic membranes is listed in Table 1. Quartz was collected from Kanpur, India. Calcium carbonate and TiO_2 were procured form Merck (I) Ltd. Fly ash was collected from Guwahati, India. All the raw materials were used as received without any further purification. Moreover, the raw materials used in this work serve for different functional attributes. Quartz increases the mechanical strength and thermal stability of the membrane. Calcium carbonate ($CaCO_3$) serves as a pore-forming agent.

2.2. Fabrication

The raw materials listed in Table 1 were mixed in a ball mill at 40 rpm for 20 min. The resulting powder was then sieved using 30 mesh standard screens and requisite amount was pressed in a hydraulic pressing machine at a pressure of 50 MPa with the help of stainless steel mould. The obtained circular disk-shaped membranes were first dried at 100˚C and then at 200˚C for 24 h in a hot air oven (make: Reico, India; model: ROV/DG). The above-controlled drying process ensures a maximum removal of moisture and also reduces any thermal stress during moisture removal. Subsequently, the membranes were sintered at 1,100˚C for 6 h in a muffle furnace (make: Lab Tech, Korea; model: LEF-115P-2) with a controlled heating rate. After sintering, the rigid and porous ceramic membranes were polished on both sides using silicon carbide abrasive paper (No. C-220) to obtain ceramic membranes with uniform surface. Then these membranes were washed with Millipore water in an ultrasonic bath [make: Elma, India; model: T460] for 15 min to remove the loose particles adhered on the surface of membranes.

3. Characterization

3.1. Particle size distribution

The particle size distribution (PSD) of the raw materials was performed by particle sizing machine, Malvern Mastersizer 2000 (APA 5005® hydro MU, Malvern Instruments, Worcestershire, UK) in wet dispersion mode.

Table 1
Composition of raw materials used for fabrication of ceramic membranes

Raw materials	Quartz (g)	$CaCO_3$ (g)	Fly ash (g)	TiO_2 (g)	$W_{TiO_2}/W_{Fly\ ash}$
Membrane, SP1	30	20	50	0	0
Membrane, SP2	30	20	40	10	0.25
Membrane, SP3	30	20	30	20	0.67
Membrane, SP4	30	20	20↓	30↑	1.50↓

3.2. X-Ray diffraction analysis

X-Ray diffraction analysis (XRD) analysis of the individual raw materials and ceramic membranes was conducted to evaluate the extent of phase transformations during sintering by Bruker AXS instrument (Karlsruhe, Germany) using CuKα (1.5406 Å) radiation operating at 40 kV and 40 mA. The patterns were acquired for 2θ range between 1˚ and 80˚ with a scan speed of 0.5˚/s.

3.3. Field emission scanning electron microscope

The images of membrane surface were taken to analyze the morphology of the membranes by field emission scanning electron microscope (FESEM, ∑IGMA, Carl Zeiss). The membrane samples were coated with gold to a thickness of approximately 150 Å. After that, FESEM images of the top surface of the membrane at different magnifications were obtained to calculate the porosity and pore size of the membrane.

3.4. Porosity

Porosity of the membrane was determined using Archimedes' principle. Firstly, the membrane was dried in a hot air oven at 110˚C for 6 h to remove complete moisture present in the membrane and its dry weight (W_D) was determined. Then, it was immersed in water for 24 h. After that, the membrane was removed and water on the outer surface was removed using tissue paper and the wet weight of the membrane (W_W) was measured. Then the membrane was immersed in water to measure the weight of the membrane when it was saturated with water (W_A). The porosity (ε) of the membrane was determined using the following relation [29,30]:

$$\varepsilon = \frac{W_W - W_D}{W_W - W_A} \quad (1)$$

where W_D is the weight of dry membrane, W_W is the weight of the membrane with pores filled with water (pores are filled with water under vacuum), and W_A is the weight of the water-saturated membrane measured in water (A refers to Archimedes).

Surface porosity of the membranes was also estimated using images obtained from FESEM. For this, ImageJ software was adopted after thresholding (threshold the pores) the 8-bit image using "Analyze particles" feature of this software. Since the pores are interconnected during thresholding, the porosity of the membranes was measured manually by choosing three rectangular sections (area) of four images of similar magnification at different locations.

3.5. Mechanical strength

The flexural strength of the membranes was tested with a three-point bending method on 55 × 5 × 5 mm rectangular bars using Universal Testing Machine (DUTT-101, M/s Deepak Polyplast, and Mumbai, India). The flexural strength was evaluated by the following expression.

$$\sigma = \frac{3Fl}{2bt^2} \quad (2)$$

where σ is the flexural strength (Pa), F is the load at the fracture point (N), l is the span length (m), b is the width of the sample (m), and t is the thickness of the sample (m).

3.6. Chemical stability

Chemical stability of the membrane was determined by subjecting the membrane individually into acid (pH 1) and alkali (pH 14) solutions. The pH of the solution was adjusted using HCl and NaOH. The stability was measured in terms of mass loss before and after corrosion. For this, the membrane was placed in acid and alkali solutions for one week at an atmospheric condition. Then the membrane was taken out from the solution, washed with Millipore water, and dried at 110˚C for 6 h. The mass loss of the membrane characterizes the chemical stability.

3.7. Hydraulic permeability and average pore size of membranes

The hydraulic permeability and average pore size of the membranes were determined by measuring their water flux using in-house made dead-end filtration setup [31,32]. Prior to the experiment, the pure water was passed through the membrane several times at higher pressure to remove any loose particles present in the pores. After that, the water flux was measured at different applied pressures (28–69 kPa). All the experiments were carried out by filling 150 ml of Millipore water in the dead-end filtration setup. After discarding the first 50 ml of water at a fixed pressure, the time required to collect next 50 ml was noted down to calculate the water flux at that particular applied pressure using the following equation:

$$J_w = \frac{Q}{A\Delta T} \tag{3}$$

where J_w is the pure water flux, Q is the volume of water permeated, A is the surface area of membrane, and ΔT is the sampling time.

The average pore size of the membrane in terms of radius is estimated by assuming the presence of cylindrical pores using the following equation deduced from Hagen–Poiseuille equation.

$$r_m = \left[\frac{8\mu l L_h}{\varepsilon}\right]^{0.5} \tag{4}$$

where r_m is the pore radius of the membrane, L_h is the hydraulic permeability of the membrane, μ is the viscosity of water, l is the pore length, and ε is the porosity of the membrane.

3.8. Separation of oil–water emulsion

The oil–water emulsion (200 mg/L) was prepared by mixing crude oil (collected from Guwahati Refinery, IOCL, India) with Millipore water in a sonicator for 15 h at room temperature (25˚C). No surfactant was added because natural surfactant present in the crude oil stabilizes the oil–water emulsion sufficiently for performing the experiments. The droplet size of the emulsion (200 mg/L) was determined using particle size analyzer (Malvern Mastersizer 2000, Model APA 5005) and the average diameter of oil droplet is found to be 6.928 μm. The prepared oil–water emulsion (concentration of 200 mg/L) was utilized for microfiltration experiments. The experiments were performed in dead-end filtration setup with varying applied pressures [30,31]. In all experiments, the feed volume of 150 mL was filled into the filtration setup. The first 10 mL of permeate was discarded and time taken for the collection of second 10 mL of permeate was noted down to calculate permeate flux. All the experiments were conducted at room temperature (25˚C) and the percentage removal (R) of oil was evaluated according to the following expression

$$R\ (\%) = \frac{C_f - C_p}{C_f} \times 100 \tag{5}$$

where C_f and C_p are the oil concentrations in the feed and permeate, respectively. The concentration of oil in permeate was evaluated using a UV–vis spectrophotometer (Spectrascan, UV 2300) at a wave length of 239 nm, where the maximum absorbance was observed.

After conducting each experiment, the membrane was cleaned with soap solution to remove the oil adhered on the surface of the membrane and flushed with water at higher pressure to obtain the original water flux. After gaining the original flux, the membrane was used for the next run.

4. Results and discussion

4.1. Particle size distribution

The PSD of the raw materials was done to get an idea of the particle size and its uniformity of the particles. The size of the raw materials determines the porosity and pore size of the sintered membrane. Pore growth mainly depends on the initial particle size of the raw materials and compaction pressure [9]. Finer particles require a relatively low temperature for sintering and conversely it results in a large transport resistance because of too small effective pore size. On the other hand, coarser particles need higher sintering temperature resulting in macroporous membranes with reduced mechanical strength [33].

The PSD of the individual raw materials and powder mixture used for the fabrication of four fly ash-based membranes (SP1–SP4) are shown in Fig. 1(a) and (b). It can be seen from Table 2 and Fig. 1(b) that the size of particles are in the ranges of 0.96–138.0 μm, 1.26–316.23 μm, 1.26–138.0 μm, and 1.26–91.2 μm for membranes SP1, SP2, SP3, and SP4, respectively. Moreover, a volume median diameter ($d_{0.5}$) of the raw material mixtures is found to be 7.3, 5.9, 5.0, and 4.8 μm for the membranes SP1, SP2, SP3, and SP4, respectively. These sized raw material mixtures would be reasonably useful for preparation of porous fly ash-based membrane with maximum porosity [33,34,35].

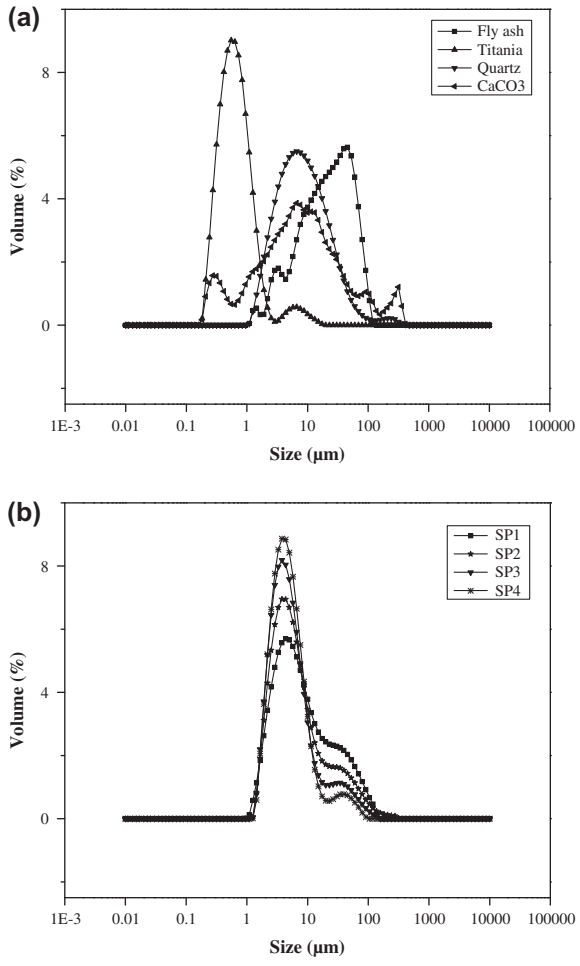

Fig. 1. PSD of (a) individual raw materials and (b) powder mixtures used to fabricate membranes (SP1–SP4).

For the powder mixtures used for fabrication of membranes (SP4–SP1), the span values are found to be in the range of 2.18–6.07. This specifies that width of the PSD offers good mixing and uniform distribution between the particles.

4.2. XRD analysis

Fig. 2 displays the XRD profiles of individual raw materials before and after calcination at 1,100°C. It is clearly seen that the chemically pure TiO_2 contains two types of crystalline phases such as anatase (major phase) and rutile (minor phase). Similar phases were also identified by Dong et al. [20] for pure TiO_2. In the fly ash, the observed crystalline phases are quartz (SiO_2) and corundum (Al_2O_3) which are consistent with the results reported by Jedidi et al. [36]. It is also noticed that in the fly ash sample, the intensity of quartz peak decreases due to the conversion of quartz to corundum at the sintering temperature. It is clearly seen from Fig. 2(b) that in comparison with the sample before calcination, the peaks corresponding to the quartz are not changed in the XRD pattern of quartz after calcination. This signifies that the quartz is not affected by the sintering temperature. According to the literature [34,35], no phase change is observed in the quartz during sintering. In addition, TGA analysis of quartz confirms that there is no significant weight loss during sintering [32,34,35]. In view of the above, it can be concluded that quartz is thermally stable at the studied sintering temperature.

The XRD reflections of the membranes (SP1–SP4) before and after sintering are presented in Fig. 3. In most cases, sintering produces a series of reactions or phase transformations that lead to the formation of new phases. As a result, the disappearance and shift in the peak positions are observed in the XRD analysis. Although many phase transformations occur during sintering of the membrane, the formation of new phase for the prepared membrane is aluminum titanate ($Al_2O_3{\cdot}TiO_2$) by reaction of rutile with corundum. During sintering, quartz reacts with rutile and converts to cristobalite and corundum [19]. The background noise in the XRD pattern of the sintered membrane suggests that there may be an existence of amorphous silica [34,37,38].

Table 2
PSD of the clay mixtures used to fabricate membranes (SP1–SP4)

Membrane	SP1	SP2	SP3	SP4
Average particle size (μm)	26.514	28.263	17.694	12.497
Span value	6.075	5.983	4.152	2.181
Volume weighted mean (μm)	16.963	14.88	10.265	7.947
Particle size range (μm)	0.955–138.038	1.259–316.228	1.259–138.038	1.259–91.201
d0.1 (μm)	2.536	2.499	2.398	2.423
d0.5 (μm)	7.282	5.888	5.017	4.847
d0.9 (μm)	46.775	37.724	23.232	12.993

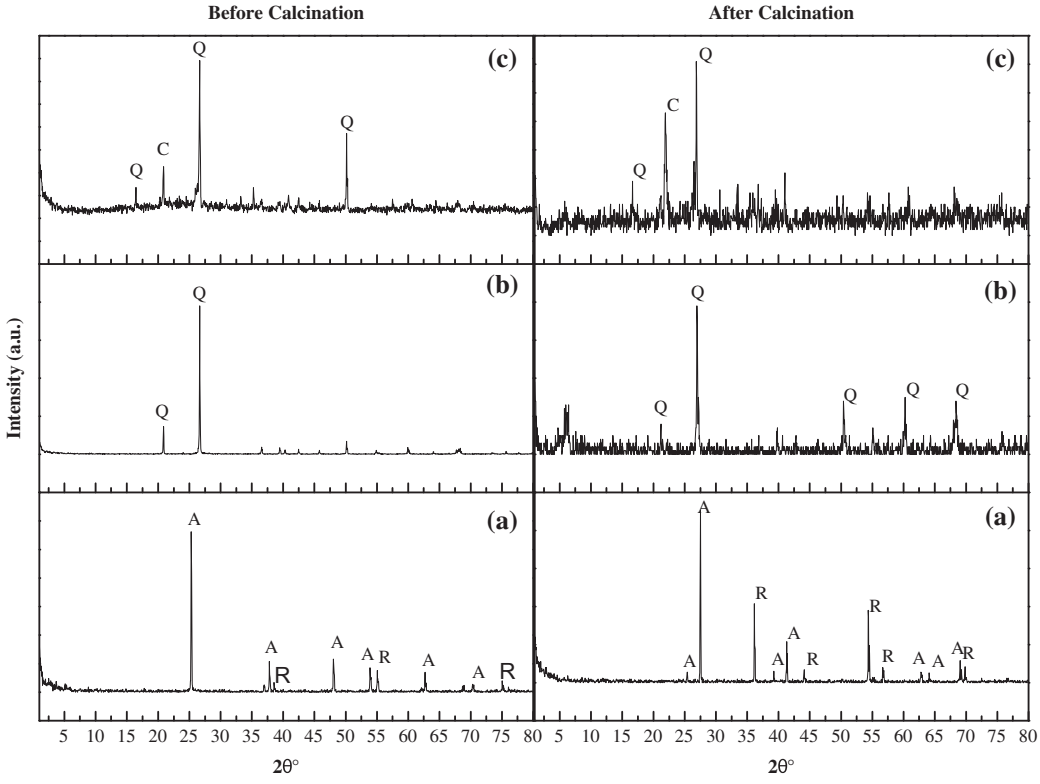

Fig. 2. XRD of raw materials (a) titanium dioxide, (b) quartz, and (c) fly ash (Q—Quartz, A—Anatase, R—Rutile, C—Corundum).

4.3. FESEM analysis

Surface morphology of the sintered membranes was studied using FESEM as depicted in Fig. 4. These images demonstrate the membrane surface with rough morphological structure. The superficial observation of the FESEM images indicates that the membranes do not have any pinholes and cracks. Moreover, the pore size distribution and average pore diameter of the membranes are estimated from FESEM micrographs using ImageJ software [39]. For each membrane, six images with various magnifications are selected for analysis to minimize the error of image analysis. The average pore size, D_{avg}, of the membrane was calculated using the following equation:

$$D_{avg} = \frac{\sum_{i=1}^{n} n_i d_i}{\sum_{i=1}^{n} n_i} \quad (6)$$

where D_{avg} is the average pore diameter (μm), n is the number of pores, and d_i is the diameter of the ith pore (μm).

The average pore size of the membranes estimated from FESEM images is found to be 3, 2.95, 2.79, and 2.28 μm for membranes SP1, SP2, SP3, and SP4, respectively. The pore size distribution of membranes is presented in Fig. 5. It is observed that the pore diameter of the membrane decreases with an increase in the TiO_2 content, which is due to the binding ability of TiO_2 during sintering. Some of the pores may even disappear during sintering. It is well documented in the literature that the membrane pore size is significantly influenced by TiO_2 content and sintering temperature [20].

4.4. Porosity

The porosity of the membranes determined by Archimedes principle and FESEM analysis is illustrated in Fig. 6. The results clearly indicate that substantial changes are observed in the porosity of the membranes when the TiO_2 content increases in the precursor formulations. In general, the porosity of the membrane mainly depends on the amount of porosifier ($CaCO_3$) and an additive (TiO_2) present in the sample. However, in this study, quantity of porosifier ($CaCO_3$), is kept constant for all membrane compositions and hence, the variation of porosity is due to the increased TiO_2 content. It is seen from the

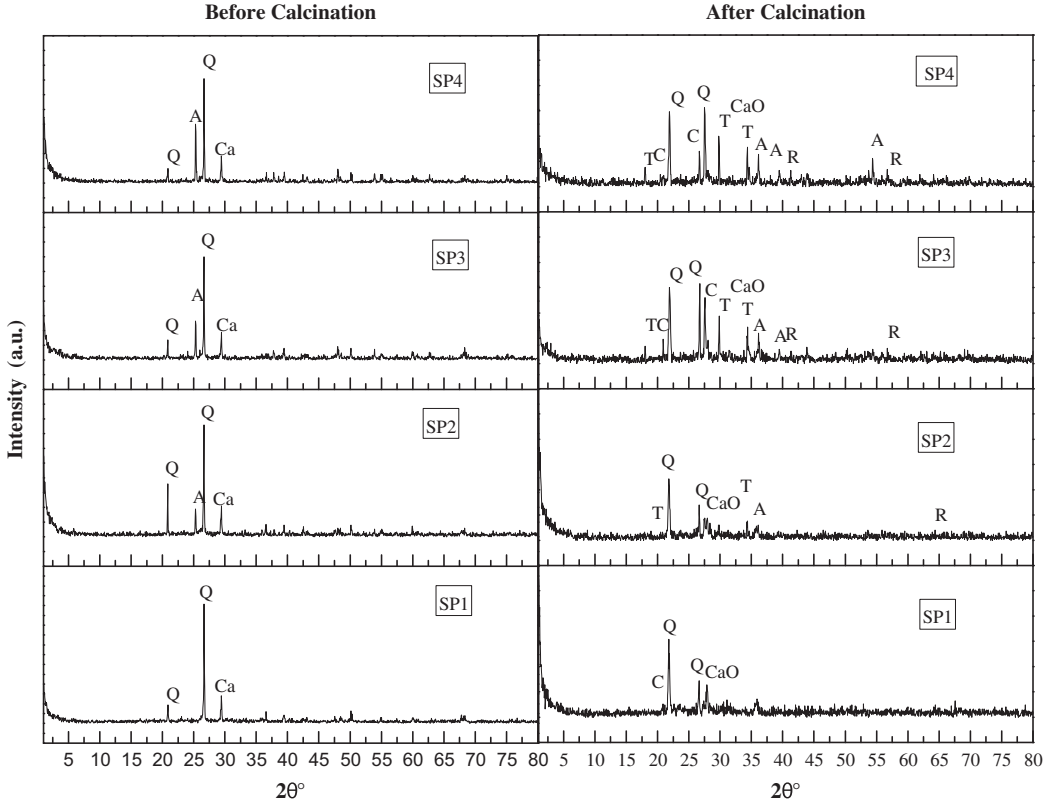

Fig. 3. XRD analysis of powder mixtures used to fabricate of membranes (SP1–SP4) (Q—Quartz, Ca—Calcium carbonate, A—Anatase, C—Corundum and Cristobalite, T—Aluminum Titanate, R—Rutile, and CaO—Calcium Oxide).

Table 1 that the domination of TiO_2 ($W_{TiO_2}/W_{fly\ ash}$) increases from 0 to 1.50. Consequently, the porosity of the membranes increases with an increase in the TiO_2 content and a maximum porosity of 48% is obtained for the SP4 membrane. It is noticed that the surface porosity of the membranes determined by FESEM analysis is higher due to difficulty in controlling the threshold of the pores of the membranes.

4.5. Chemical stability

The chemical stability of the membranes was evaluated in terms of mass loss after keeping the membrane in contact with acid and alkali solutions individually. As the TiO_2 content increases, the weight loss of the membranes due to the corrosion of acid decreases from 6 to 2% as depicted in Fig. 7. The weight loss of the membrane due to alkali is found to be around 1% for all the membranes. The results reveal that the membranes exhibit better corrosion resistance in both acidic medium and basic medium. The obtained results are comparable with cordierite [40] and alumino silicate microfiltration membranes [41].

4.6. Mechanical strength

Fig. 8 demonstrates that with increasing TiO_2 content in the precursor formulations, the flexural strength of the membranes increases from 6.02 to 13.82 MPa. Similar observation was also reported by Dong et al. [20]. In general, calcium carbonate ($CaCO_3$) is used as a porosifier as well as a sintering aid. Besides, the flexural strength of the membrane primarily depends on the amount of sintering aid present in the precursor sample [17,42,43]. However, in this study, the amount of $CaCO_3$ is kept constant for all the membrane formulations. Hence, the enhanced flexural strength of the membrane is due to the increased densification with higher amount of TiO_2 at the sintering temperature (1,100˚C) [20].

4.7. Hydraulic permeability and average pore size of membranes

All the prepared membranes were characterized for their hydraulic permeability. Pure water flux was measured by applying different pressures ranging between 28 and 69 kPa as depicted in Fig. 9. It is observed that the flux of the membranes depends on

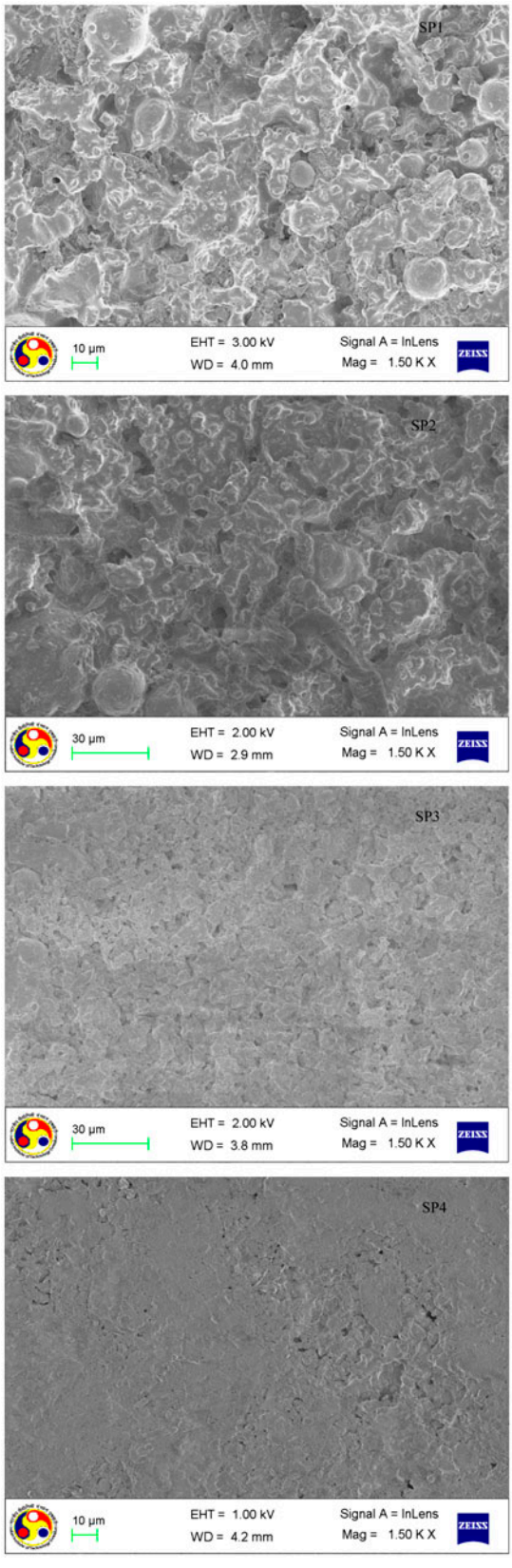

Fig. 4. FESEM images of the membranes (SP1–SP4).

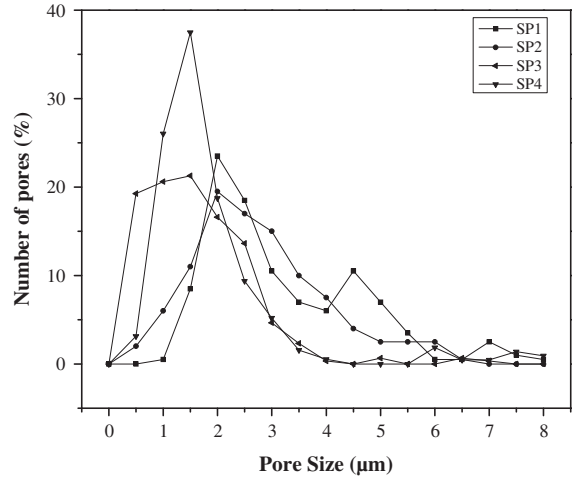

Fig. 5. Pore size distribution analysis of the membranes (SP1–SP4) from FESEM images.

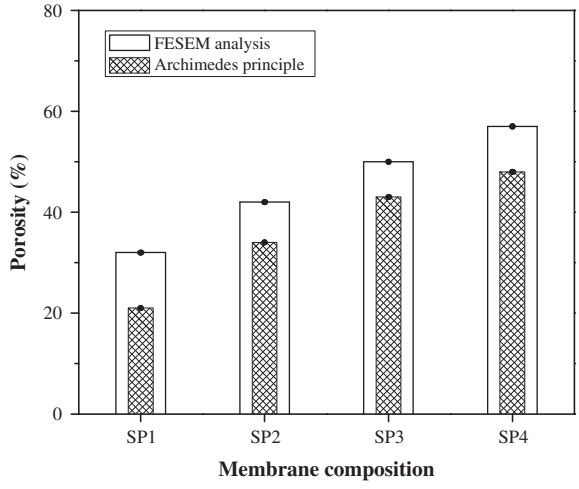

Fig. 6. Porosity of membranes from FESEM analysis and Archimedes principle.

the applied pressure and also increases with an increase in the applied pressure. The hydraulic permeability of the membranes is estimated to be 1.58×10^{-8}, 1.14×10^{-8}, 0.87×10^{-8}, and 0.63×10^{-8} (m^3/m^2s Pa) for the membranes SP1, SP2, SP3, and SP4, respectively. The average pore diameter of the membranes calculated from hydraulic permeability data is found to be 2.97, 1.77, 1.57, and 1.32 µm for the membrane SP1, SP2, SP3, and SP4, respectively. The reduction in the pore size and pure water flux of the membranes with increasing TiO_2 content in the precursors is due to better densification of the membranes. The pore size of the ceramic membranes measured by FESEM analysis is slightly higher than those calculated from pure water permeability data.

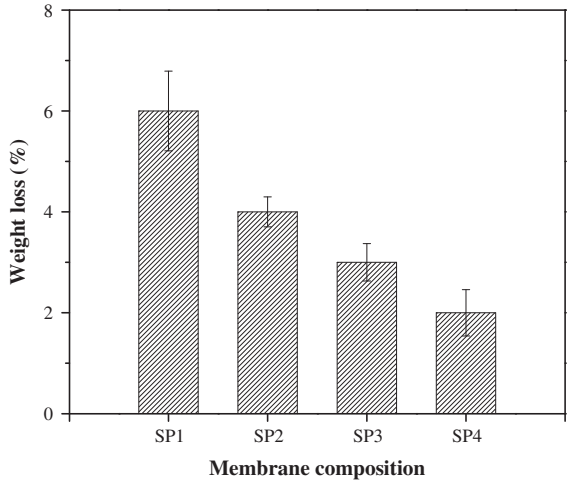

Fig. 7. Chemical stability of the membranes (SP1–SP4) in acid.

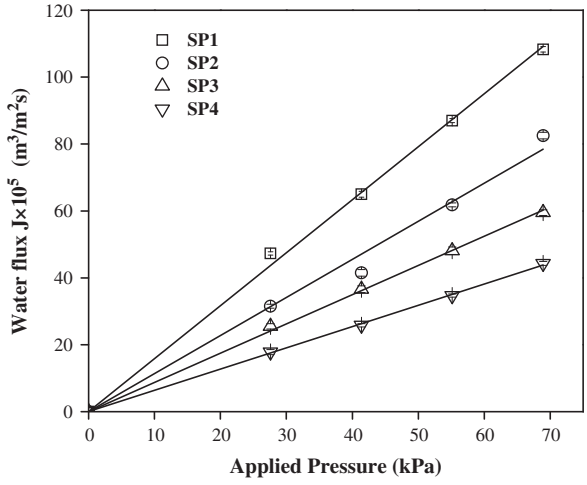

Fig. 9. Variation of pure water flux of the membranes at different applied pressures.

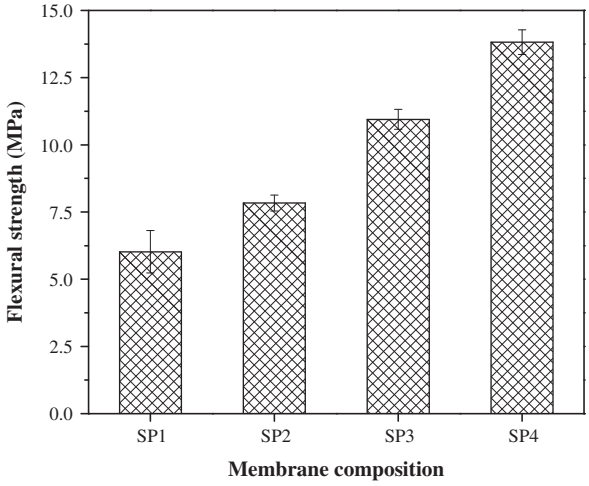

Fig. 8. Flexural strength of the membranes (SP1–SP4).

FESEM tends to overestimate the pore size as it can only assess the pore diameter at the surface of the membrane and some of the pores may be dead-end pores (not through pores). The pore size obtained from water permeability data corresponds to a minimal size of the pore constriction through which water passes and is smaller than the surface pore size. Thus the pore size obtained from water permeability is more accurate than FESEM analysis.

4.8. Separation of oil–water emulsion

Among the prepared membranes, the lowest pore size membrane (SP4) was tested for separation of oil–water emulsion. Fig. 10 illustrates the variation of the permeate flux and percentage removal of oil with various applied pressures (69–345 kPa) for the initial oil concentration of 200 mg/L. As expected, the removal of oil decreases with an increase in the applied pressure. This is due to the fact that the higher pressure enhances the wetting and coalescence of oil droplets and this would enforce the oil droplets to pass through the membrane along with the permeate. The observed results are consistent with the results reported in the literature [27,44]. The maximum rejection of 99.2% is observed at a lower applied pressure of 69 kPa. As the applied pressure increases from 69 to 345 kPa, the permeate flux also increases due to enhancement of the driving force across the membrane. A large difference between permeate flux

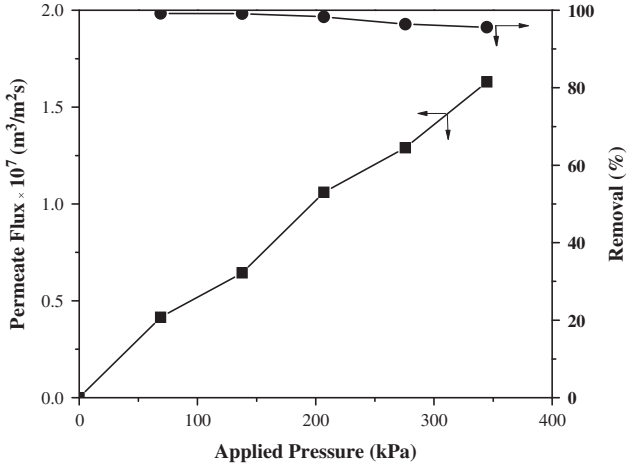

Fig. 10. Variation of permeate flux and percentage removal of oil at different applied pressures for SP4 membrane.

Table 3
Comparison of oil removal percentage of fabricated membrane with other membranes

Membrane/support material	Mean pore size	Feed concentration (mg/L)	Removal (%)	References
α-Al_2O_3/α-Al_2O_3	1.0 μm	5,000	94.3	Yang et al. [45]
α-Al_2O_3/α-Al_2O_3	0.2 μm	5,000	99.9	Yang et al. [45]
ZrO_2/α-Al_2O_3	0.2 μm	5,000	99.8	Yang et al. [45]
NaA zeolite/α-Al_2O_3	1.2 μm	100	98.8	Cui et al. [46]
α-Al_2O_3	2.1 μm	100	55.0	Cui et al. [46]
NaA zeolite/α-Al_2O_3	0.4 μm	100	99.4	Cui et al. [46]
Al_2O_3	0.16 μm	600–11,000	98.0	Cui et al. [46]
α-Al_2O_3	0.1 μm	150	61.4	Ebrahimi et al. [47]
TiO_2/TiO_2	1,000 Da	565	99.5	Ebrahimi et al. [47]
Membrane, SP4	1.32 μm	200	99.2	Present study

and pure water flux under same condition is observed for the studied membrane (SP4) on account of pore blocking and concentration polarization (see Figs. 9 and 10). From an industrial application's point of view, the membranes should possess higher removal efficiency with good permeate flux. Hence, it can be concluded that the prepared membrane, SP4, displays better rejection (99.2–95.6%) of oil with permeate flux. In comparison with other membranes (see Table 3), the performance of the prepared membrane in terms of rejection and permeate flux, is comparable or even better than those reported in the literature. It can be concluded from Table 3 that the membrane (SP4) prepared from fly ash is useful for treating oily wastewater in the form of oil-in-water emulsion.

4.9. Cost estimation

Based on the retail cost of the raw materials, the average cost of the ceramic membranes is estimated as Rs. 3, 5, 6.5, and 8.5 per circular-shaped membrane for SP1, SP2, SP3, and SP4, respectively, that correspond to 15–40 ($/m^2) as listed in Table 4. The cost of the prepared membranes is comparable and even lower than the membranes reported in the literature [48–52]. It is worth to mention that the cost of the ceramic membranes prepared by Emani et al. [48], Vasanth et al. [49], Nandi et al. [50] and Mittal et al. [52] is 78, 67, 130, and 34 ($/m^2), respectively. Moreover, cost of the inorganic membranes is projected to be around 500–1,000 ($/m^2) [53–55]. The cost of the commercial membrane made of α-Al_2O_3 is reported to be 989–1,220 ($/m^2) [56].

Cost is always considered as a massive apprehension in the membrane process, which is mainly from energy consumption and membrane replacement. The use of conventional membranes in wastewater treatment requires high energy input in order to keep constant efficiency due to lower membrane permeability. Generally, membranes made of clay-based raw materials possess higher permeability than conventional membranes; as a result, lower cost on energy. Currently, natural clays and fly ash are most preferred membrane materials when compared with other materials because of their low cost. Typically, the membrane process using alumina and zirconia-based membranes

Table 4
Cost estimation of membranes (SP1–SP4)

Raw materials	Unit price (Rs./kg)	Amount of raw materials used for the fabrication of one membrane (kg)	Cost estimated for the fabrication of one membrane (Rs.)			
			Membrane, SP1	Membrane, SP2	Membrane, SP3	Membrane, SP4
Quartz	10.00	7.50×10^{-3}	0.075	0.075	0.075	0.075
Calcium carbonate	520	5.00×10^{-3}	2.6	2.6	2.6	2.6
Fly ash	28.0	12.5×10^{-3}	0.35	0.28	0.21	0.14
Titania	720	2.5×10^{-3}	–	1.8	3.6	5.4
Raw materials cost for one membrane fabrication			3.02	4.76	6.48	8.22
Cost of one ceramic membrane of 5 mm thickness and 63 mm diameter (rounded value)			3/membrane	5/membrane	6.5/membrane	8.5/membrane
Estimated raw materials cost per unit area of the fabricated membrane			963/m^2 (15 $/m^2)	1,605/m^2 (25 $/m^2)	2086/m^2 (33 $/m^2)	2,567/m^2 (40 $/m^2)

is more expensive than those using clay-based membranes because of the costly raw materials. On the contrary, fly ash is rather cost-effective compared to conventional membranes. In addition, enhanced anti-fouling ability of the clay-based membranes extends the back-flushing interval and membrane life span that also increase the price gap between the clay membranes and commercial membranes.

5. Conclusions

A series of low-cost ceramic membranes have been successfully prepared using different compositions of raw materials by uniaxial dry compaction method. The membrane porosities are found to be 21, 34, 43, and 48 for the SP1, SP2, SP3, and SP4 membranes, respectively. The prepared membranes with various compositions offer good mechanical strength (6.02–13.82 MPa). The weight loss of the membranes (SP1–SP4) in acid and alkali solutions are found to be 6–2% and 1%, respectively, indicating that these membranes are more stable in both acidic medium and basic medium. The average pore sizes of the membranes calculated from water permeability data are found to be 2.97, 1.77, 1.57, and 1.32 μm for membranes SP1, SP2, SP3, and SP4, respectively. The performance of the fabricated membrane (SP4) is demonstrated by the separation of oil from oil–water emulsion. The maximum removal of oil is observed to be 99.2% with permeate flux of 4.1×10^{-8} (m^3/m^2s) at an applied pressure of 69 kPa for the initial oil concentration of 200 mg/L. Based on the cost of raw materials, cost of the membranes is estimated to be around 15–40 ($\$/m^2$).

Acknowledgments

We would like to thank the Central Instrument Facility, IIT Guwahati for helping to perform FESEM analysis. XRD, used in this work, was financially supported by a FIST grant (SR/FST/ETII-028/2010) from the Department of Science and Technology (DST), Government of India.

List of symbols

ε — the porosity of the membrane
W_D — the weight of dry membrane (g)
W_W — weight of the membrane with pores filled with water (pores are filled with water under vacuum) (g)
W_A — the weight of the membrane saturated with water measured in water (A refers to Archimedes) (g)
σ — the flexural strength (Pa)
F — the load at the fracture point (N)
l — the span length (m)
b — the width of the sample (m)
t — the thickness of the sample (m)
J_w — the pure water flux (m^3/m^2 s)
Q — the volume of water permeated (m^3)
A — the surface area of membrane (m^2)
ΔT — the sampling time (s)
r_m — the pore radius of the membrane (μm)
L_h — the hydraulic permeability of the membrane (m^3/m^2s Pa)
μ — the viscosity of water (Pa s)
ΔP — the transmembrane pressure drop across the membrane (kPa)
l — pore length (m)
R — rejection of oil (%)
C_f — the oil concentration in the feed (mg/L)
C_p — the oil Concentration in the permeate (mg/L)
D_{avg} — the average pore diameter (μm)
n — the number of pores
d_i — the diameter of the ith pore (μm)

References

[1] Y. Yoshino, T. Suzuki, B.N. Nair, H. Taguchi, N. Itoh, Development of tubular substrates, silica based membranes and membrane modules for hydrogen separation at high temperature, J. Membr. Sci. 267 (2005) 8–17.
[2] J.M. Benito, A. Conesa, F. Rubio, M.A. Rodríguez, Preparation and characterization of tubular ceramic membranes for treatment of oil emulsions, J. Eur. Ceram. Soc. 25 (2005) 1895–1903.
[3] Y.S. Lin, A.J. Burggraaf, Preparation and characterization of high-temperature thermally stable alumina composite membrane, J. Am. Ceram. Soc. 74 (1991) 219–224.
[4] D.S. Bae, D.S. Cheong, K.S. Han, S.H. Choi, Fabrication and microstructure of Al_2O_3–TiO_2 composite membranes with ultrafine pores, Ceram. Int. 24 (1998) 25–30.
[5] G. Pugazhenthi, S. Sachan, N. Kishore, A. Kumar, Separation of chromium (VI) using modified ultrafiltration charged carbon membrane and its mathematical modeling, J. Membr. Sci. 254 (2005) 229–239.
[6] S. Judd, B. Jefferson, Membranes for Industrial Wastewater Recovery and Re-use, Elsevier, Oxford, 2003.
[7] K.A. DeFriend, M.R. Wiesner, A.R. Barron, Alumina and aluminate ultrafiltration membranes derived from alumina nanoparticles, J. Membr. Sci. 224 (2003) 11–28.
[8] Y.H. Wang, T.F. Tian, X.Q. Liu, G.Y. Meng, Titania membrane preparation with chemical stability for very hash environments applications, J. Membr. Sci. 280 (2006) 261–269.
[9] T. Tsuru, Inorganic porous membranes for liquid phase separation, Sep. Purif. Methods 30 (2001) 191–220.
[10] C. Falamaki, M.S. Afarani, A. Aghaie, Initial sintering stage pore growth mechanism applied to the

manufacture of ceramic membrane supports, J. Eur. Ceram. Soc. 24 (2004) 2285–2292.
[11] N. Saffaj, H. Loukili, S.A. Younssi, A. Albizane, M. Bouhria, M. Persin, A. Larbot, Filtration of solution containing heavy metals and dyes by means of ultrafiltration membranes deposited on support made of Moroccan clay, Desalination 168 (2004) 301–306
[12] N. Saffaj, M. Persin, S.A. Younsi, A. Albizane, M. Cretin, A. Larbot, Elaboration and characterization of microfiltration and ultrafiltration membranes deposited on raw support prepared from natural Moroccan clay: Application to filtration of solution containing dyes and salts, Appl. Clay. Sci. 31 (2006) 110–119.
[13] N. Saffaj, M. Persin, S. A. Younssi, A. Albizane, M. Bouhria, H. Loukili, H. Dach, A. Larbot, Removal of salts and dyes by low $ZnAl_2O_4$–TiO_2 ultra-filtration membrane deposited on support made from raw clay, Sep. Purif. Technol. 47 (2005) 36–42.
[14] S. Khemakhem, A. Larbot, R.B. Amara, Study of performances of ceramic microfiltration membrane from Tunisian clay applied to cuttlefish effluents treatment, Desalination 200 (2006) 307–309.
[15] M.R. Weir, E. Rutinduka, C. Detellier, C.Y. Feng, Q. Wang, T. Matsuura, R. Le VanMao, Fabrication, characterization and preliminary testing of all-inorganic ultrafiltration membranes composed entirely of a naturally occurring sepiolite clay mineral, J. Membr. Sci. 182 (2001) 41–50.
[16] K. Khider, D.E. Akretche, A. Larbot, Purification of water effluent from a milk factory by ultrafiltration using Algerian clay support, Desalination 167 (2004) 147–151.
[17] F. Bouzerara, A. Harabi, S. Achour, A. Larbot, Porous ceramic supports for membranes prepared from kaolin and doloma mixtures, J. Eur. Ceram. Soc. 26 (2006) 1663–1671.
[18] A. Majouli, S. Tahiri, S. Alami Younssi, H. Loukili, A. Albizane, Elaboration of new tubular ceramic membrane from local Moroccan perlite for microfiltration process. Application to treatment of industrial wastewater, Ceram. Int. 38 (2012) 4295–4303.
[19] I. Jedidi, S. Khemakhem, A. Larbot, A.R. Ben, Elaboration and characterization of fly ash based mineral supports for microfiltration and ultra filtration membranes, Ceram. Int. 35 (2009) 2747–2753.
[20] Y. Dong, S. Hampshire, J. Zhou, B. Lin, Z. Ji, X. Zhang, G. Meng, Recycling of fly ash for preparing porous mullite membrane supports with titania addition, J. Hazard. Mater. 180 (2010) 173–180.
[21] J. Fang, G.T. Qin, W. Wei, X.Q. Zhao, Preparation and characterization of tubular supported ceramic microfiltration membranes from fly ash, Sep. Purif. Technol. 80 (2011) 585–591.
[22] C. Xia, M. Liu, A simple and cost-effective approach to fabrication of dense ceramic membranes on porous substrates, J. Am. Ceram. Soc. 84 (2001) 1903–1905.
[23] A. Ezzati, E. Gorouhi, T. Mohammadi, Separation of water in oil emulsion using microfiltration, Desalination 189 (2006) 87–91.
[24] T. Mohammadi, A. Pak, M. Karbassian, M. Golshan, Effect of operating conditions on microfiltration of an oil-water emulsion by a kaolin membrane, Desalination 168 (2004) 201–205.
[25] I.W. Cumming, R.G. Holdich, I.D. Smith, The rejection of oil by microfiltration of a stabilized kerosene/water emulsion, J. Membr. Sci. 169 (2000) 147–155.
[26] F.L. Hua, Y.F. Tsang, Y.J. Wang, S.Y. Chan, H. Chua, S.N. Sin, Performance study of ceramic microfiltration membrane for oily wastewater treatment, Chem. Eng. J. 128 (2007) 169–175.
[27] S. Abadi, M. Sebzari, M. Hemati, F. Rekabdar, T. Mohammadi, Ceramic membrane performance in microfiltration of oily wastewater, Desalination 265 (2011) 222–228.
[28] J. Zhou, Q. Chang, Y. Wang, J. Wang, G. Meng, Separation of stable oil–water emulsion by the hydrophilic nano-sized ZrO_2 modified Al_2O_3 microfiltration membrane, Sep. Purif. Technol. 75 (2010) 243–248.
[29] P. Monash, G. Pugazhenthi, Effect of TiO_2 addition on the fabrication of ceramic membrane supports: A study on the separation of oil droplets and bovine serum albumin (BSA) from its solution, Desalination 279 (2011) 104–114.
[30] D. Laux, J.Y. Ferrandis, J. Bentama, M. Rguiti, Ultrasonic investigation of ceramic clay membranes, Appl. Clay Sci. 32 (2005) 82–86.
[31] D. Vasanth, G. Pugazhenthi, R. Uppaluri, Fabrication of low cost ceramic microfiltration membranes for separation of oil and bacteria from its solution, J. Membr. Sci. 379 (2011) 154–163.
[32] D. Vasanth, G. Pugazhenthi, R. Uppaluri, Performance of low cost ceramic microfiltration membranes for the treatment of oil-in-water emulsions, Sep. Sci. Technol. 48 (2013) 849–858.
[33] Y.H. Wang, Y. Zhang, X.Q. Liu, G.Y. Meng, Sol-coated preparation and characterization of macroporous α-Al_2O_3 membrane support, J. Sol–Gel Sci. Technol. 41 (2007) 267–275.
[34] P. Monash, G. Pugazhenthi, Development of ceramic supports derived from low cost clays for membrane applications and its optimization based on sintering temperature, Int. J. Appl. Ceram. Technol. 8 (2011) 227–238.
[35] D. Vasanth, R. Uppaluri, G. Pugazhenthi, Influence of sintering temperature on the properties of porous ceramic support prepared by uniaxial dry compaction method using low-cost raw materials for membrane applications, Sep. Sci. Technol. 46 (2011) 1241–1249.
[36] I. Jedidi, S. Khemakhem, S. Saïdi, A. Larbot, N.E. Elloumi-Ammar, A. Fourati, A. Charfi, A.B. Salah, R.B. Amar, Preparation of a new ceramic microfiltration membrane from mineral coal fly ash: Application to the treatment of the textile dying effluents, Powder. Technol. 208 (2011) 427–432.
[37] A. Gualtieri, M. Bellotto, G. Artioli, S.M. Clark, Kinetic study of the kaolinite-mullite reaction sequence. Part II: Mullite formation, Phys. Chem. Miner. 22 (1995) 215–222.
[38] G. Cultrone, C. Rodriguez-Navarro, E. Sebastian, O. Cazalla, M.J. De La Torre, Carbonate and silicate phase reactions during ceramic firing, Eur. J. Mineral. 13 (2001) 621–634.

[39] Open source software provided by National Institute of Health (NIH). Available from: http://rsbweb.nih.gov/ij/download.html.
[40] Y.C. Dong, X.Q. Liu, Q.L. Ma, G.Y. Meng, Preparation of cordierite-based porous ceramic micro-filtration membranes using waste fly ash as the main raw material, J. Membr. Sci. 285 (2006) 173–181.
[41] M.C. Almandoz, J. Marchese, P. Prádanos, L. Palacio, A. Hernández, Preparation and characterization of non-supported microfiltration membranes from aluminosilicates, J. Membr. Sci. 241 (2004) 95–103.
[42] B. Boudaira, A. Harabia, F. Bouzerara, S. Condom, Preparation and characterization of microfiltration membranes and their supports using kaolin (DD2) and $CaCO_3$, Desalin. Water Treat. 9 (2009) 142–148.
[43] C. Falamaki, M. Naimi, A. Aghaie, Dual behavior of $CaCO_3$ as a porosifier and sintering aid in the manufacture of alumina membrane/catalyst supports, J. Eur. Ceram. Soc. 24 (2004) 3195–3201.
[44] T.C Arnot, R.W. Field, A.B. Koltuniewicz, Cross-flow and dead-end microfiltration of oily-water emulsions part II. Mechanisms and modelling of flux decline, J. Membr. Sci. 169 (2000) 1–15.
[45] C. Yang, G. Zhang, N. Xu, J. Shi, Preparation and application in oil–water separation of ZrO_2/α-Al_2O_3 MF membrane, J. Membr. Sci. 142 (1998) 235–243.
[46] J. Cui, X. Zhang, H. Liu, S. Liu, K.L. Yeung, Preparation and application of zeolite/ceramic microfiltration membranes for treatment of oil contaminated water, J. Membr. Sci. 325 (2008) 420–426.
[47] M. Ebrahimi, D. Willershausen, K.S. Ashaghi, L. Engel, L. Placido, P. Mund, P. Bolduan, P. Czermak, Investigations on the use of different ceramic membranes for efficient oil-field produced water treatment, Desalination 250 (2010) 991–996.
[48] S. Emani, R. Uppaluri, M.K. Purkait, Preparation and characterization of low cost ceramic membranes for mosambi juice clarification, Desalination 317 (2013) 32–40.
[49] D. Vasanth, R. Uppaluri, G. Pugazhenthi, Influence of sintering temperature on the properties of porous ceramic support prepared by uniaxial dry compaction method using low-cost raw materials for membrane applications, Sep. Sci. Technol. 46 (2011) 1241–1249.
[50] B. K. Nandi, R. Uppaluriand M. K.Purkait, Identification of optimal membrane morphological parameters during microfiltration of mosambi juice using low cost ceramic membranes, LWT – Food Sci. Technol. 44 (2011) 214 –223.
[51] S. Jana, M.K. Purkait, K. Mohanty, Preparation and characterization of low-cost ceramic microfiltration membranes for the removal of chromate from aqueous solutions, Appl. Clay Sci. 47 (2010) 317–324.
[52] P. Mittal, S. Jana, K. Mohanty, Synthesis of low-cost hydrophilic ceramic–polymeric composite membrane for treatment of oily wastewater, Desalination 282 (2011) 54–62.
[53] W.J. Koros, R. Mahajan, Pushing the limits on possibilities for large scale gas separation: Which strategies? J. Membr. Sci. 175 (2000) 181–196.
[54] S.P. Nunes, K.V. Peinemann, Membrane Technology in the Chemical Industry, first ed., Wiley, New York, NY, 2001.
[55] Ceramiques Techniques & Industrielles, SA, France, 2007. Available from: http://perso.orange.fr/ctisa.
[56] H. Krawczyk, A.S. Jönsson, The influence of feed flow channel diameter on frictional pressure drop, membrane performance and process cost in full-scale tubular membranes, Chem. Eng. Res. Des. 92 (2014) 174–180.